NANO LETTERS

pubs.acs.org/NanoLett Letter

Stabilizing a Lithium Metal Battery by an In Situ Li_2S-modified Interfacial Layer via Amorphous-Sulfide Composite Solid Electrolyte

Chen Lai, Chengyong Shu, Wei Li, Liu Wang, Xiaowei Wang, Tianran Zhang, Xuesong Yin, Iqbal Ahmad, Mingtao Li, Xiaolu Tian, Pu Yang, Wei Tang,* Naihua Miao,* and Guangyuan Wesley Zheng*

Cite This: *Nano Lett.* 2020, 20, 8273−8281 Read Online

ABSTRACT: A novel strategy has been proposed to produce in situ Li_2S at the interfacial layer between lithium anode and the solid electrolyte, by using an amorphous-sulfide−LiTFSI−poly-(vinylidene difluoride) (PVDF) composite solid electrolyte (SLCSE). Besides retarding the decomposition of PVDF in CSE, the Li_2S-modified interfacial layer (SMIL) also improves the wettability between lithium metal and SLCSE which in turn optimizes the lithium deposition process. Our density functional theory calculation results reveal that the migration energy barrier of Li passing through SMIL is much lower than that of Li passing through LiF-modified interfacial layer (FMIL) formed from the decomposition of PVDF. The as-prepared SLCSE shows a Li ionic transference number of 0.44 and Li ion conductivity of 3.42×10^{-4} S/cm at room temperature, and the Li||SLCSE||$LiFePO_4$ cell exhibits an outstanding rate performance with a capacity of 153, 144, 131, and 101 mAh/g at a current density of 0.05, 0.10, 0.25, and 0.50 mA/cm^2, respectively.

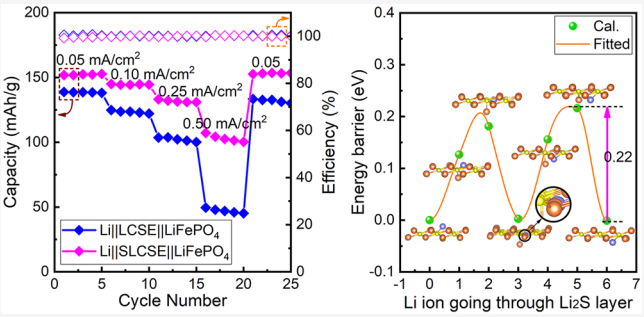

KEYWORDS: *interfacial layer, composite solid electrolyte, lithium metal batteries, amorphous sulfide*

INTRODUCTION

Recently, the urgency for higher energy density has increased with demand of electrical vehicles and large-scale electric power storage systems. The Li metal anode with a high theoretical specific capacity (3860 mAh/g) and ultranegative potential (−3.040 V vs the standard hydrogen electrode) is an ultimate choice for next generation lithium metal batteries (LMBs) to achieve the high-energy-density goal. However, serious safety issues caused by liquid flammable electrolyte leakage and lithium dendrite short circuiting in conventional organic liquid electrolyte LMBs are the major problems that urgently need to be addressed first. In this respect, solid-state electrolytes are considered as highly desired materials for replacing state-of-the-art liquid flammable electrolytes and enabling the use of lithium metal as an anode, which can well address safety issues and provide higher energy density.[1,2]

On the basis of their components, solid-state electrolytes are classified into polymer electrolyte, inorganic ceramic electrolyte, and composite solid electrolyte (CSE) categories. Polymer electrolyte, which is composed of poly(vinylidene difluoride) (PVDF) or poly(ethylene oxide) (PEO) and lithium salt, such as $LiPF_6$, $LiBF_4$, $LiN(SO_2CF_3)_2$ (LiTFSI), and $LiN(SO_2F)_2$ (LiFSI), draws a lot of attention for its low cost, high flexibility, and easy scalability in recent years.[3−8] However, the moderate ion conductivity and low mechanical strength of polymer electrolytes make it difficult to meet the requirements of practical applications.[9] Despite the high modulus and excellent ionic conductivity of inorganic ceramic electrolytes,[10−12] the poor interfacial contact and large electrolyte−electrode interfacial resistance between inorganic electrolyte and the electrode result in rapid failure of battery cycling.[13−17] To address these issues, interfacial architectures are proposed to increase the wettability between inorganic ceramic electrolytes and electrodes.[18−20] For example, by coating a layer of PEO-based polymer on both sides of $Li_7La_3Zr_2O_{12}$ (LLZO) electrolyte, the interface polarization of a $LiFePO_4$ full battery decreases to ∼30 mV when serving at 90 °C.[21] Though the interfacial contact ability is significantly improved by the artificial interlayer, it induces extra interfacial resistance and makes interfacial evolution and Li ion transportation modes more complicated. In this case, one of the alternative choices is the use of a CSE that is composed of

Received: August 20, 2020
Revised: October 19, 2020
Published: October 27, 2020

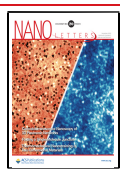

https://dx.doi.org/10.1021/acs.nanolett.0c03395
Nano Lett. 2020, 20, 8273−8281

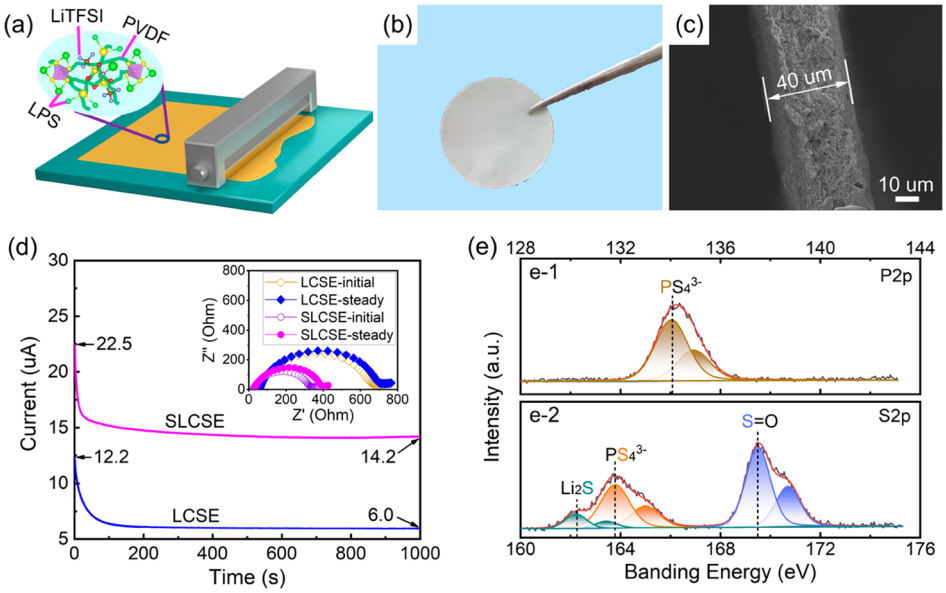

Figure 1. Preparation and characterization of LCSE and SLCSE. (a) The preparation scheme of SLCSE; (b) the appearance of SLCSE; (c) the section of SLCSE; (d) the Nyquist plots of Li||LCSE||Li and Li||SLCSE||Li symmetrical cells before and after the polarization; and the chronoamperometry profiles under a polarization voltage of 10 mV, with (e) the spectra of P 2p (up) and S 2p (under) of pristine SLCSE.

inorganic ceramic electrolyte and polymer electrolyte, which combines the merits of an inorganic ceramic electrolyte and polymer electrolyte, such as their high mechanical strength, satisfying ion conductivity, excellent flexibility, and good wettability with electrodes.[22] Lithium dendrites can grow into the holes and grain boundaries of inorganic ceramic electrolytes, as well as in the soft phase of CSE,[23−25] risking short circuiting of LMBs. In this case, Li dendrites could not be well suppressed merely by CSE. Therefore, one of the critical obstacles for practical application of CSE is how to prevent lithium dendrite penetrating through the CSE.[26−29]

Various proofs have demonstrated that the lithium dendrite growth is attributed to the nonuniform plating and stripping of Li on the surface of the Li metal anode.[30] Instead of exhaustedly suppressing Li dendrite growth by the high mechanical module of a solid-state electrolyte, the in situ construction of a solid-electrolyte interphase that is well compatible to electrodes and contributes to the uniform plating and stripping of Li is a promising and advantageous strategy to serve the purpose well.[31−33] For example, by constructing an artificial solid-electrolyte interphase (SEI) composed of Cu_3N nanoparticles and styrene butadiene rubber, uniform Li-ion flux was realized by in situ formation of a Li_3N layer on the surface of the Li metal anode, helping to suppress Li dendrite formation.[34] However, another critical issue that cannot be ignored is the inevitable dehydrofluorination process of PVDF polymer during Li stripping−plating experiments, leading to the failure of CSE.[32] The side reaction between PVDF and Li metal provides electrons for the reduction of Li ions when Li ions migrate through CSE, which consequently aggravates the uneven plating and striping of Li.[32,35] Therefore, preventing the decompositions of CSE is as essentially important as suppressing the formation of lithium dendrites for improving the safety and lifespan of LMBs.

Herein, a new strategy was proposed to construct a Li_2S-modified interfacial layer (SMIL) in situ on the surface of a Li metal anode to homogenize the plating and striping of Li and to mitigate the decomposition of PVDF in SLCSE. By constructing such a SMIL on the surface of the Li metal anode, the decomposition of PVDF in SLCSE is significantly mitigated. Moreover, the SMIL is beneficial to improve the uniformity of Li deposition and the reversible capacity owing to the remarkable improvement of the wettability between lithium metal and SLCSE. Consequently, the formation of SMIL enables the Li||SLCSE||$LiFePO_4$ cell to exhibit a high capacity of 153, 144, 131, and 101 mAh/g at 0.05, 0.10, 0.25, and 0.50 mA/cm^2, respectively, as well as a good capacity retention of 99.5% at the 150th cycle under 0.05 mA/cm^2 (vs the 20th cycle).

■ RESULTS AND DISCUSSION

In our present work, amorphous $3Li_2S{\cdot}2P_2S_5$ (hereafter abbreviated as LPS) compound powder was fabricated by the solvent method. The as-prepared LPS powder with the particle size distributed in dozens to hundreds of nanometers (Figure S1) was mainly composed of an amorphous phase and a trace amount of Li_3PS_4 and Li_2S crystalline phases (Figure S2). Using the LPS as a filler, we prepared a flexible sulfide−LiTFSI−PVDF composite solid-electrolyte-based (hereafter abbreviated as SLCSE) film by doctor blading (Figure 1a). Upon solvent evaporation, the typical thickness of flexible SLCSE is around 40 μm (Figure 1b, c). The LiTFSI−PVDF composite solid electrolyte (hereafter abbreviated as LCSE) without LPS was also prepared with similar processes for comparison. As shown in Figure S3, the SLCSE filled with LPS powders possesses a remarkable flat surface, which may render intimate contact with the lithium metal anode. As demonstrated in Figure 1d, the Li ion transference number of SLCSE is about 0.44, which is much higher than that of LCSE (0.16). Moreover, the SLCSE shows a much lower interface resistance than the LCSE (the inset of Figure 1d, Table S1), which should be attributed to the better wettability between lithium metal and the SLCSE electrolyte. The Li ion conductivity values of LCSE and SLCSE are determined by the EIS plots of SS||CSE||SS (SS = stainless steel) (Figure S4). Based on the equivalent circuit model,[36] the Li ion conductivities of LCSE

https://dx.doi.org/10.1021/acs.nanolett.0c03395
Nano Lett. 2020, 20, 8273−8281

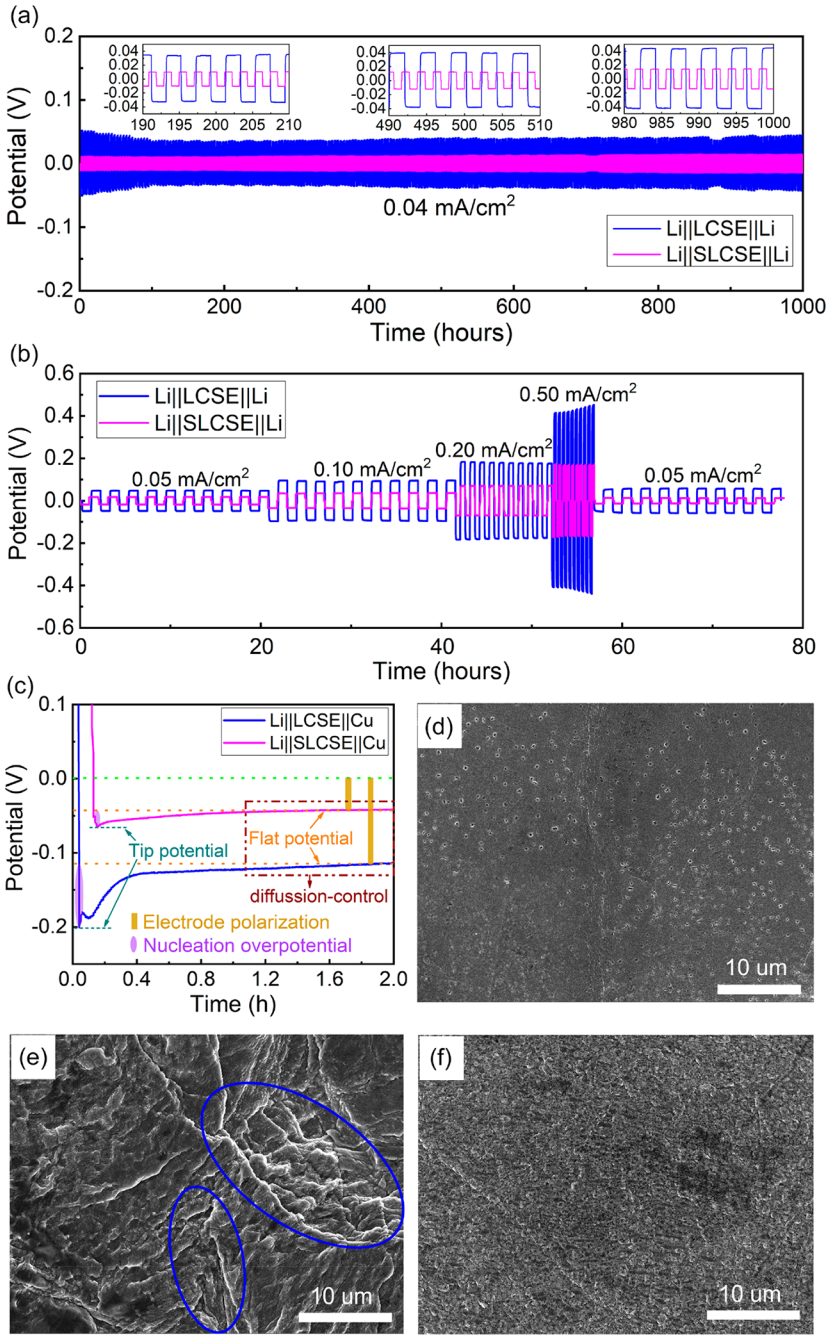

Figure 2. Plating and striping performance of Li. (a) Cycling performances of Li||SLCSE/LCSE||Li symmetrical cells; (b) rate performances of Li||SLCSE/LCSE||Li symmetric cells; surface morphologies of the (c) plating profile of Li in Li||LCSE||Cu and Li||SLCSE||Cu semisymmetrical cells; and the SEM images of (d) pristine Li metal and the Li metal anode after 10 cycles in the (e) Li||LCSE||Cu semisymmetrical cell and (f) Li||SLCSE||Cu semisymmetric cell.

and SLCSE at room temperature were calculated to be 2.40 × 10^{-4} S/cm and 3.42 × 10^{-4} S/cm, respectively. It has been reported that the Li ion migration in CSE could proceed both at the ceramic|polymer interface and at the interior of the ceramic.[37−39] Therefore, the LPS dispersed in SLCSE is essential to increase the Li ion conductivity and transference number. Since the LPS is amorphous, the chemical species in LPS were determined by the deconvoluted XPS data of phosphorus and sulfur. As shown in Figure 1e, a double peak locating at 134.0 and 134.8 eV is assigned to the P 2p of PS_4^{3-}. The binding energies of S 2p located at 162.2, 163.8, and 169.5 eV are attributed to Li_2S, PS_4^{3-}, and S═O ($TFSI^-$),[40,41] respectively (Figures 1e and 2). It is demonstrated that the LPS in SLCSE is mainly composed of amorphous Li_2S and Li_3PS_4.

To investigate the stability and wettability between SLCSE and Li metal, Li||SLCSE/LCSE||Li symmetrical cells were assembled. Figure 2a displays the cycling performance of Li||SLCSE or LCSE||Li symmetric cells that were periodically charged and discharged for 1 h each at a current density of 0.04 mA/cm^2 at 25 °C. The polarization voltage of the Li||SLCSE||Li cell is about 15 mV, while the polarization voltage of the Li||LCSE||Li symmetric cell reaches up to 35 mV. The polarization voltage in the Li||SLCSE||Li symmetric cell increases by only 4

https://dx.doi.org/10.1021/acs.nanolett.0c03395
Nano Lett. 2020, 20, 8273−8281

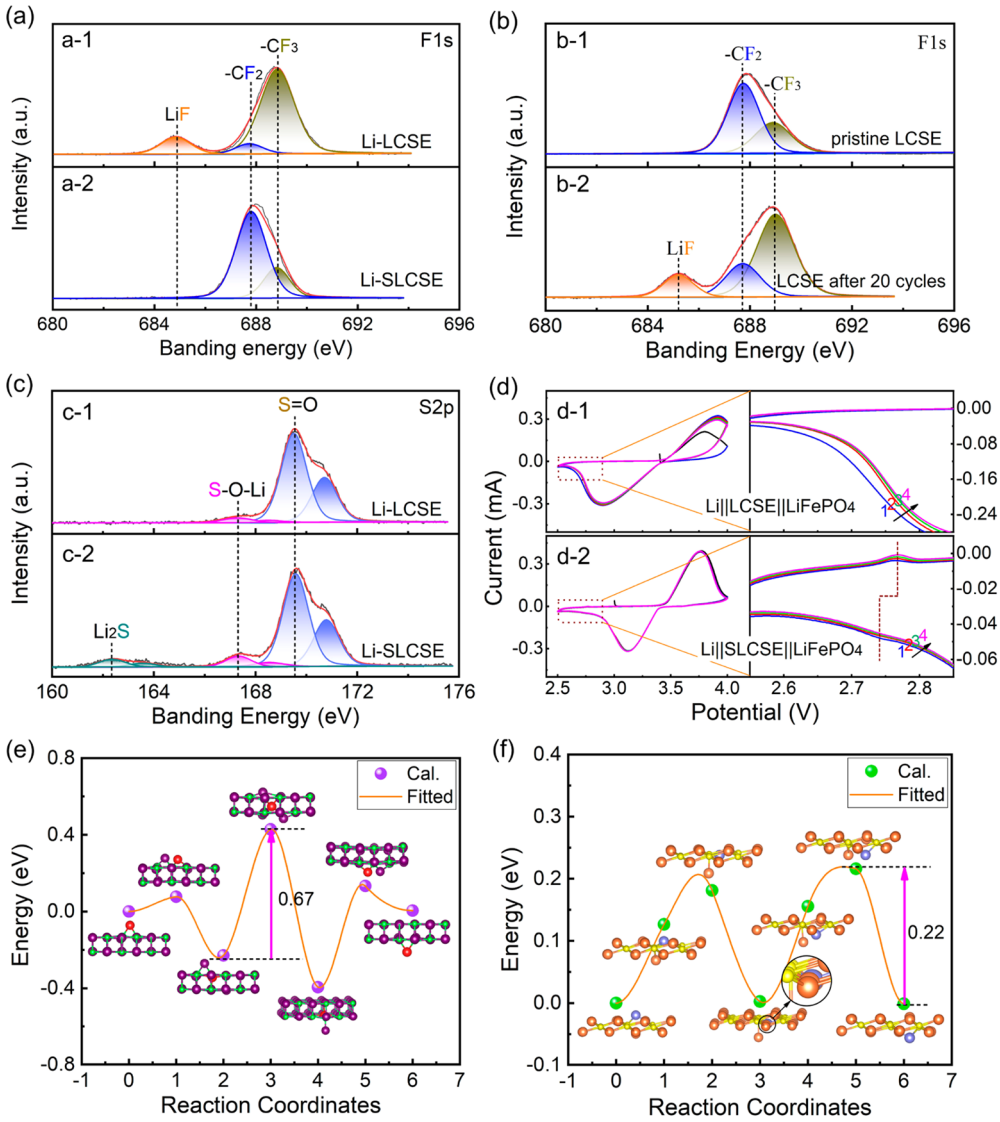

Figure 3. Studies of the interfacial layer. (a) The XPS data of F 1s of Li-LCSE (a-1) and Li-SLCSE (a-2) in Li||$LiFePO_4$ full cells after 20 cycles; (b) the XPS data of F 1s of pristine LCSE (b-1) and LCSE in the Li||LCSE||$LiFePO_4$ cell after 20 cycles (b-2); (c) the XPS data of S 2p of Li-LCSE (c-1) and Li-SLCSE (c-2) in Li||$LiFePO_4$ full cells after 20 cycles; (d) the 1st−4th cyclic voltammogram curves of the Li||LCSE||$LiFePO_4$ cell (d-1) and Li||SLCSE||$LiFePO_4$ cell (d-2); and the migration energy barrier of Li ions passing through the (e) LiF layer and (f) Li_2S layer.

mV when cycling from the 200th hour to the 1000th hour, which is only about half of that in Li||LCSE||Li symmetric cells. As it is shown in Figure 2b, the plating/stripping curves of Li||SLCSE||Li are stable as the charge/discharge current density increases from 0.05 to 0.50 mA/cm^2. However, the overpotential of the Li||LCSE||Li cell is two times higher than that of the Li||SLCSE||Li cell at the same operating current density. Reasonably, the lower polarization voltage is attributed to the lower interfacial resistance, stemming from the better wettability between lithium metal and SLCSE. This deduction can be confirmed by the values of electrode polarization voltage in Li||LCSE||Cu and Li||SLCSE||Cu semisymmetric cells (Figure 2c), which is controlled by the diffusion behavior of Li ion in the electrolyte.[42] The Li nucleation barrier, referring to the wettability, can be reflected by the plating overpotential at the initial stage of Li deposition.[43] Figure 2c illustrates the plating profile of Li deposition on the surface of copper foil in Li||LCSE or SLCSE||Cu cells. It can be seen that the SLCSE not only provides a lower nucleation overpotential for Li plating than that of LCSE but also exhibits a lower electrode polarization. The accumulated capacity loss plots of Li||LCSE||Cu and Li||SLCSE||Cu indicate that the wettability of SLCSE is higher than that of LCSE (Figure S5). Figure 2d shows the SEM image of pristine Li metal. Figure 2e and 2f display the microscopy images of Li metal anode in Li||LCSE||Cu and Li||SLCSE||Cu semisymmetric cells after 10 cycles of charging−discharging at 0.05 mA/cm^2, respectively. The bright part on the surface of Li-LCSE (Figure 2e) is suggested to be dead lithium and SEI (circled by a blue line). Apparently, the morphology of Li deposition on the surface of the Li metal anode in the Li||SLCSE||Cu semisymmetric cell is hemispherical, while the morphology of Li deposition on the surface of the Li metal anode in the Li||LCSE||Cu semisymmetric cell is random and rough. This phenomenon can also be observed on the surface of Li metal anode in the Li||LCSE||$LiFePO_4$ full cell after cycling at 0.50 mA/cm^2 (Figure S6). It is reasonable to believe that the flat surface of the Li metal anode and low electrode polarization of SLCSE derive from uniform plating

https://dx.doi.org/10.1021/acs.nanolett.0c03395
Nano Lett. 2020, 20, 8273−8281

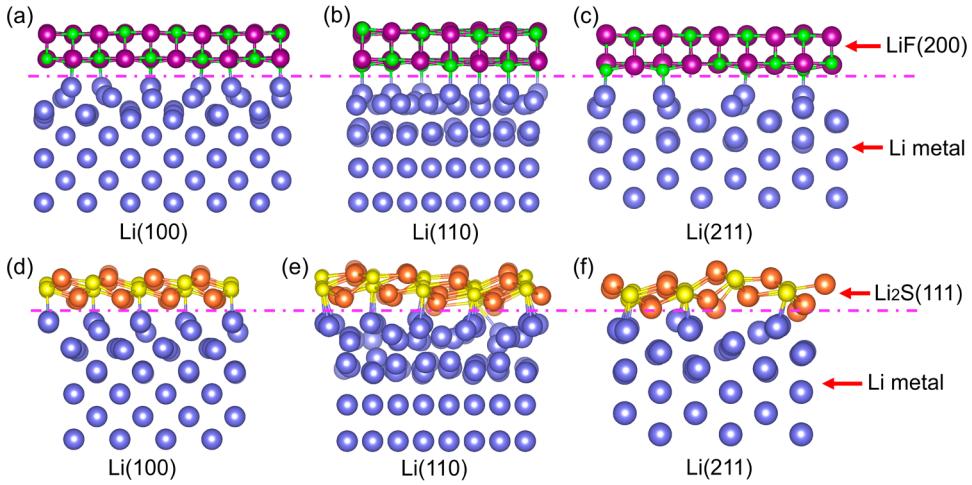

Figure 4. Optimized structure of the interfaces: (a) Li(100)|LiF, (b) Li(110)|LiF, (c) Li(211)|LiF, (d) Li(100)|Li_2S, (e) Li(110)|Li_2S, and (f) Li(211)|Li_2S.

and stripping of Li during repeated charging−discharging, which is closely related to the interfacial layer.[44,45]

In order to understand the interfacial layers of Li|LCSE and Li|SLCSE, ex situ X-ray photoelectron spectroscopy (XPS) was employed to ascertain the electrochemical evolution of the interfacial layers (Figure 3). A SMIL was in situ formed on the surface of the Li metal anode in the Li||SLCSE||$LiFePO_4$ cell, which is contributed to retard the decomposition of PVDF of SLCSE. Figure 3a-1 and Figure 3a-2 show the deconvoluted F 1s spectra on the surface of the Li metal anode in the Li||LCSE||$LiFePO_4$ cell (Li-LCSE) and the Li||SLCSE||$LiFePO_4$ cell (Li-SLCSE) after 20 cycles, respectively. As shown in Figure 3a-1, the binding energies of the F 1s spectra locating at 684.9, 687.8, and 688.9 eV are attributed to LiF, $-CF_2$, and $-CF_3$, respectively.[32,35] The F 1s spectra of $-CF_2$ and $-CF_3$ stem from PVDF and $TFSI^-$, while the fluorine source of LiF may derive from the decompositions of PVDF and LiTFSI during repeated charging−discharging.[32,35,46] In order to further study whether the fluorine source of LiF originates from the decomposition of PVDF or LiTFSI,[46] the XPS spectra of F 1s of pristine LCSE and LCSE in Li||LCSE||$LiFePO_4$ after 20 cycles were carefully investigated, as shown in Figure 3b. According to the F 1s signal in LCSE before and after 20 cycles (Figure 3b-1−2), the relative intensity of the F 1s signal belonging to $-CF_2$ in LCSE is subjected to significant change, which indicates that the fluorine source of LiF is dominantly attributed to the decomposition of PVDF in the present work. Notably, no F 1s spectra of LiF are observed on the surface of Li-SLCSE, demonstrating that the defluorination of PVDF and LiTFSI is retarded in the Li||SLCSE||$LiFePO_4$ cell. This deduction can be confirmed by the relative intensity ratio of $-CF_2/-CF_3$ in SLCSE before and after 20 cycles (Figure S7). Figure 3c-1 and Figure 3c-2 show the deconvoluted S 2p spectra on the surface of Li-LCSE and Li-SLCSE, respectively. Two S 2p double peaks presented at 169.4 and 170.5 evV and 167.3 and 168.5 eV are attributed to S═O and S—O—Li, respectively. The S 2p spectra of S═O are owed to pristine $TFSI^-$, while the S 2p spectra of S—O—Li derives from S═O after lithiation. On the surface of Li-SLCSE, apart from the S 2p spectra of S═O and S—O—Li, another S 2p double peak is presented at 162.3 and 163.5 eV, which is attributed to the S 2p spectrum of in situ formed Li_2S (Figure 3c-2). These values of binding energy agree well with already reported XPS results of Li_2S.[38,39] It is noteworthy that no S 2p spectra of PS_4^{3-} (LPS) presents on the surface of Li-SLCSE, which indicates that the performance of the interfacial layer is mainly tailored by the SMIL. The difference of sulfide-based species presented on Li-SLCSE and SLCSE after 20 cycles reveals that the chemical species on the Li-SLCSE belong to SEI rather than SLCSE (Figure S8). Except for the P 2p spectra of PS_4^{3-}, no extra P 2p signal was observed on the surfaces of SLCSE after 20 cycles, indicating the stability of PS_4^{3+} in SLCSE (Figure S9). The decompositions of PVDF and LiTFSI lead to partial blocking of the lithium transportation pathway of LCSE, inducing nonuniform Li plating and stripping.[47] The absence of LiF on the surface of the Li-SLCSE anode and the lower polarization voltage in the Li||SLCSE||Li symmetric cell (Figure 2b) demonstrate that the SMIL on the surface of the Li metal anode not only helps to mitigate the decomposition of PVDF but also contributes to the wettability between SLCSE and the Li metal anode. Therefore, the cyclic voltammetries (CV) performed on Li||LCSE||$LiFePO_4$ and Li||SLCSE||$LiFePO_4$ cells are used to investigate the formation of SMIL (Figure 3d). As shown in Figure 3d, compared to the CV curves of the Li||LCSE||$LiFePO_4$ cell (Figure 3d-1), an extra pair of reduction−oxidation peaks locating at around 2.75 V were observed in the CV curves of the Li||LCSE||$LiFePO_4$ cell (Figure 3d-2), which can be attributed to the electrochemical reaction of formation of SMIL. Evidently, the SMIL derived from LPS on the surface of Li-SLCSE is induced by the electrochemical process during repeated charging−discharging cycles. The Li_2S in SMIL can be formed not only by the chemical diffusion from SLCSE but also from the electrochemical reaction during charging/discharging cycling.[48] It has been reported that the poor chemical stability of PVDF toward Li metal results in the uneven formation of LiF[49] and topically provides electrons for the reduction of Li ions on the surface of the Li-LCSE anode,[50,51] which further leads to the uncontrolled growth of Li dendrites.[52] Notably, the behavior of Li deposition is also significantly affected by the kinetics of Li ion migration in interfacial layers formed on the surface of the Li metal anode.[42] In our present work, the dominated differences of chemicals on the surface of Li metal anode are LiF and Li_2S. This can be confirmed by the XPS profile of Li 1s on the surface of Li-LCSE and Li-SLCSE after 20 cycles (Figure S10). Therefore,

https://dx.doi.org/10.1021/acs.nanolett.0c03395
Nano Lett. 2020, 20, 8273−8281

Li_2S and LiF involved in the interfacial layer are the main reason for the improved electrochemical performance. Though bulk Li_2S shows low Li ion conductivity at room temperature,[53] the nanoscale Li_2S SEI exhibits high Li ion conductivity.[54] For these reasons, density functional theory (DFT) calculations were performed to understand the migration behavior of Li when passing through LiF and Li_2S layers. As illustrated in Figure 3e and 3f, the calculated migration energy barrier of Li ions passing through LiF layer is 0.67 eV, while it is 0.22 eV for that in Li_2S layer. Obviously, this means that the Li ion conductivity of SMIL is much higher than that of FMIL, which benefits the uniformity of Li plating and stripping and consequently helps to suppress the growth of Li dendrites. The migration energy barriers of Li in Li ionic conductors reported by DFT calculations and experiments are collected in Figure S11. It can be seen that the calculated migration energy barrier of Li in the Li_2S layer (0.22 eV) is close to that previously reported of Li in bulk β-Li_3PS_4 (~0.20 eV) and $Li_7P_3S_{11}$ (0.24 eV),[55,56] verifying the high Li ion conductivity of the Li_2S layer.

It is well known that crystal growth is closely related to the surface energy of the crystal plane. Generally, a crystal grows along the plane with lower surface energy. In order to have a further understanding on the effect of LiF and Li_2S layers on the performance of Li plating/stripping, DFT calculations were performed to study the formation energy of Li, Li|LiF, and Li|Li_2S sufaces/interfaces (Figure 4 and Table 1). It can be seen that the values of formation energies of pristine Li(100), Li(110), and Li(211) surfaces are 0.47, 0.50, and 0.55 J/m^2, respectively. These data are close to previously reported results,[57] indicating the reliability of our calculation method. Whereas, the formation energies of interface Li(100)|LiF (Figure 4a), Li(110)|LiF (Figure 4b), and Li(211)|LiF (Figure 4c) and of Li(100)|Li_2S (Figure 4d), Li(110)|Li_2S (Figure 4e), and Li(211)|Li_2S (Figure 4f) are −0.084, −0.078, −0.096 J/m^2 and −0.39, −0.29, −0.44 J/m^2, respectively. Obviously, the formation energies of Li(100), Li(110), and Li(211) surfaces are positive, while the corresponding formation energies of Li|LiF or Li|Li_2S interfaces are negative. This implies that the interface of Li|LiF and Li|Li_2S can be spontaneously formed when LiF or Li_2S is present. However, with the much lower formation energy of the interface, the Li|Li_2S interface is energetically preferable to form on the Li metal anode than that of the Li|LiF interface when both LiF and Li_2S are present. These calculations verify that Li_2S layer exhibits a better wettability to Li metal than that of LiF layer, which could be confirmed by the interfacial resistance of Li||LCSE||Li at various cycles (Figure S12) and the SEM images of the cross section of the interfacial layer between the Li metal anode and LCSE/SLCSE (Figure S13). As shown in Figure S12, the interfacial resistance of Li||SLCSE||Li decreases significantly after 100 charging−discharging cycles, attributed to the presence of SMIL, while the interfacial resistance of Li||LCSE||Li is subjected to a decrease at the 50th cycle and then an increase at the 100th cycle due to the decomposition of PVDF. Compared with LCSE, as shown in Figure S13, the more intimate contact between Li metal anode and SLCSE implies the higher wettability of SLCSE. On the other hand, the positive surface energies of the Li(100), Li(110), and Li(211) suggest that additional energies are necessary when forming these surface. The higher the surface energy is, the more additional energy is needed. Thus, Li atoms prefer to deposit on the crystal plane with lower surface energy, which may lead to the growth of Li dendrites on the surface of a pristine Li metal anode.[58] Whereas, the formation energy of the Li|LiF (or Li|Li_2S) interface needs to be overcome when Li dendrites pierce through LiF layer (or Li_2S layer). Compared with the Li|LiF interface, the lower formation energy of the Li|Li_2S interface indicates that the dendrite suppression ability of Li_2S layer is higher than that of LiF layer. The theoretical results are in excellent agreement with the experimental SEM images of the Li metal anode (Figure 2e, 2f). On the other hand, the lower formation energy of the Li|Li_2S interface illustrates that the wettability of Li_2S layer to Li metal anode is higher than that of LiF layer to Li metal anode. Further, the better wettability will result in a higher contact area of the interface and a lower interfacial polarization voltage, which also contribute to improve the capacity and rate performance of LMBs.

Table 1. Formation Energy of the Li Surface and Li|LiF and Li|Li_2S Interfaces

formation energy [J/m^2]	Li	Li|LiF	Li|Li_2S
Li(100)	0.47	−0.084	−0.39
Li(110)	0.50	−0.078	−0.29
Li(211)	0.55	−0.096	−0.44

To examine the effect of in situ SMIL on the performance of Li metal batteries, Li||SLCSE||$LiFePO_4$ cells were assembled along with a Li||LCSE||$LiFePO_4$ full cell. Figure 5a shows the galvanostatic cycling performance of Li||LCSE||$LiFePO_4$ and Li||SLCSE||$LiFePO_4$ cells at the current density of 0.05 mA/cm^2 at 25 °C. The lifetime of the Li||SLCSE||$LiFePO_4$ full cell is more than 150 cycles with a capacity retention up to 99.5% (vs the 20th cycle), while the failure of the Li||LCSE||$LiFePO_4$ full cell induced by parasitic reaction is observed at the 95th cycle. As shown in the galvanostatic charge−discharge profile of the 50th and 80th cycles (Figure 5b), the polarization voltage of the Li||SLCSE||$LiFePO_4$ cell is obviously smaller than that of the Li||LCSE||$LiFePO_4$ cell. As it is shown in Figure 5c, the discharge capacity at 0.05, 0.10, 0.25, and 0.50 mA/cm^2 is 153, 144, 131, and 101 mAh/g for the Li||SLCSE||$LiFePO_4$ cell and 138, 123, 102, and 47 mAh/g for the Li||LCSE||$LiFePO_4$ cell, respectively, indicating the superior rate capability of the Li||SLCSE||$LiFePO_4$ cell over that of the Li||LCSE||$LiFePO_4$ cell. Moreover, as it is shown in Figure 5d, the polarization of the Li||SLCSE||$LiFePO_4$ cell at high current (0.50 mA/cm^2) is much smaller than that of the Li||LCSE||$LiFePO_4$ cell. The capacity and polarization in the Li||SLCSE||$LiFePO_4$ cell are significantly improved owing to the SMIL. The electrochemical performance agrees very well with the observations in the lithium symmetric cells and the calculated prediction.

In summary, a new $3Li_2S{\cdot}2P_2S_5$−LiTFSI−PVDF-based composite solid electrolyte (SLCSE) was proposed to modify the wettability between highly reactive lithium metal and composited solid electrolytes as well as to mitigate the uncontrollable decomposition of PVDF at the interface. Along with a high ionic conductivity of 3.42×10^{-4} S/cm and high ionic transference number of 0.44 at room temperature, the SLCSE helps to in situ construct a Li_2S-modified interfacial layer between lithium metal and the solid electrolyte, which provides benefits to improve the wettability and stability of the interfacial layer. Our DFT calculations reveal that the migration barrier energy of Li passing through

https://dx.doi.org/10.1021/acs.nanolett.0c03395
Nano Lett. 2020, 20, 8273−8281

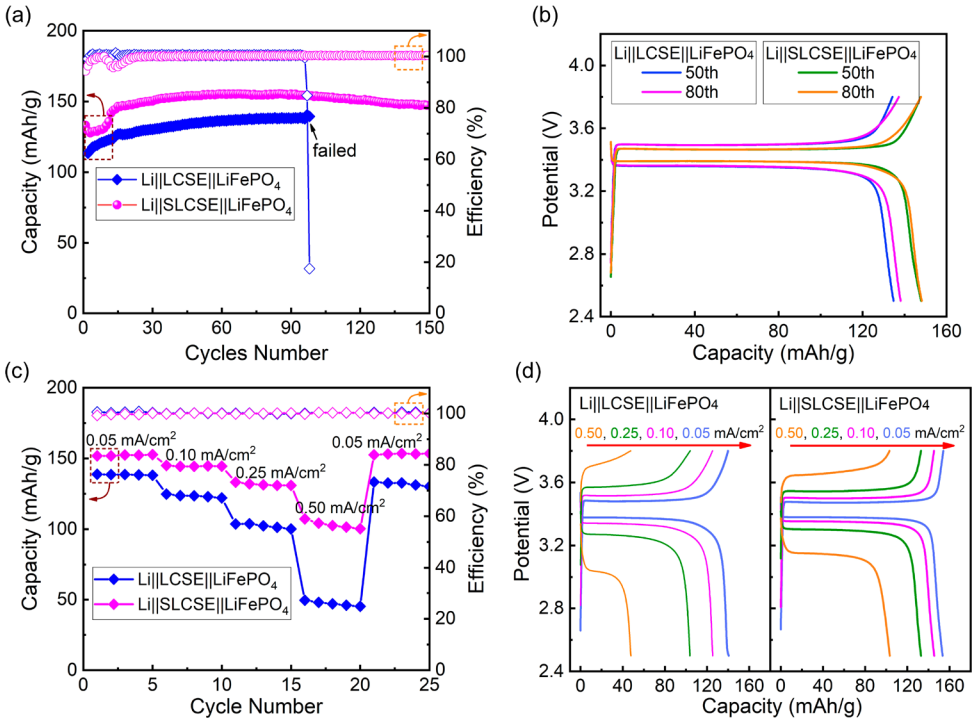

Figure 5. Electrochemical performance of Li||LCSE||$LiFePO_4$ and Li||SLCSE||$LiFePO_4$ cells. (a) Cycling performance at the current density of 0.05 mA/cm^2 at 25 °C; (b) rate performance at different current densities; (c) the galvanostatic charge−discharge profile of the 50th and 80th cycle at 0.05 mA/cm^2; and (d) the galvanostatic charge−discharge profile at different charging−discharging current densities.

Li_2S layer is much lower than that of Li passing through LiF layer. Additionally, the formation energy of the Li|Li_2S interface is much lower than that of the Li|LiF interface and the pristine Li metal surface, indicating the higher wettability to the Li metal and better suppression ability to Li dendrites. As expected, the Li||SLCSE||$LiFePO_4$ cell shows an excellent rate capability with a capacity of 153, 144, 131, and 101 mAh/g at 0.05, 0.10, 0.25, and 0.50 mA/cm^2, respectively, and excellent cyclability with a capacity retention of 99.5% at the 150th cycle under 0.05 mA/cm^2 (vs the 20th cycle). Our findings provide a new strategy to address the critical interfacial challenge in solid-state LMBs.

■ ASSOCIATED CONTENT

Supporting Information

The Supporting Information is available free of charge at https://pubs.acs.org/doi/10.1021/acs.nanolett.0c03395.

Additional details involving characterization and fabrication of samples and simulations (PDF)

■ AUTHOR INFORMATION

Corresponding Authors

Wei Tang − *School of Chemical Engineering and Technology, Xi'an Jiaotong University, Xi'an 710049, People's Republic of China; State Key Laboratory of Space Power-Sources Technology, Shanghai Institute of Space Power-Sources, Shanghai 200245, People's Republic of China;* Email: tangw2018@xjtu.edu.cn

Naihua Miao − *School of Materials Science and Engineering, Beihang University, Beijing 100191, People's Republic of China;* Email: nhmiao@buaa.edu.cn

Guangyuan Wesley Zheng − *Department of Chemical and Biomolecular Engineering, National University of Singapore, Singapore 117585 Singapore; Institute of Materials Research and Engineering, Singapore 138634 Singapore;* orcid.org/0000-0003-0286-5908; Email: chezg@nus.edu.sg, wesley-zheng@imre.a-star.edu.sg

Authors

Chen Lai − *School of Chemical Engineering and Technology, Xi'an Jiaotong University, Xi'an 710049, People's Republic of China; Department of Chemical and Biomolecular Engineering, National University of Singapore, Singapore 117585 Singapore;* orcid.org/0000-0002-8482-7800

Chengyong Shu − *School of Chemical Engineering and Technology, Xi'an Jiaotong University, Xi'an 710049, People's Republic of China*

Wei Li − *School of Materials Science and Engineering, Beihang University, Beijing 100191, People's Republic of China*

Liu Wang − *Department of Chemical and Biomolecular Engineering, National University of Singapore, Singapore 117585 Singapore;* orcid.org/0000-0002-9562-8700

Xiaowei Wang − *NUS Graduate School for Integrative Sciences and Engineering, National University of Singapore, Singapore 119077 Singapore*

Tianran Zhang − *Department of Chemical and Biomolecular Engineering, National University of Singapore, Singapore 117585 Singapore;* orcid.org/0000-0003-2837-4971

Xuesong Yin − *Institute of Materials Research and Engineering, Singapore 138634 Singapore;* orcid.org/0000-0003-1335-8506

Iqbal Ahmad − *School of Chemical Engineering and Technology, Xi'an Jiaotong University, Xi'an 710049, People's Republic of China*

Mingtao Li − *School of Chemical Engineering and Technology, Xi'an Jiaotong University, Xi'an 710049, People's Republic of China*

https://dx.doi.org/10.1021/acs.nanolett.0c03395
Nano Lett. 2020, 20, 8273−8281

Xiaolu Tian − *School of Chemical Engineering and Technology, Xi'an Jiaotong University, Xi'an 710049, People's Republic of China*

Pu Yang − *School of Chemical Engineering and Technology, Xi'an Jiaotong University, Xi'an 710049, People's Republic of China*

Complete contact information is available at:
https://pubs.acs.org/10.1021/acs.nanolett.0c03395

Notes

The authors declare no competing financial interest.

■ ACKNOWLEDGMENTS

This work was financially supported by the Chinese Postdoctoral Science Foundation (2019M653601), the National Nature Science Foundation of China (21905220, 61874146, and 21803005), the Fundamental Research Funds for the Young Talent Support Plan of Xi'an Jiaotong University (HG6J003), a grant from Shaanxi Joint Laboratory of Graphene (NPU), and the 1000-Plan Program of Shaanxi Province. G.W.Z. and W.L. acknowledge support by Singapore Ministry of Education Academic Research Fund Tier 1 R-279-000-550-133. We thank Phai Ann Chia, Rajamohan S'O.K. Suppiah, Zhicheng Liu, and Zeliang Yuan at the Department of Chemical and Biomolecular Engineering of the National University of Singapore for the SEM analysis, XRD test, and XPS characterization. We also thank Instrument Analysis Center of Xi'an Jiaotong University and Neware Technology Limited.

■ REFERENCES

(1) Ji, X. L. A paradigm of storage batteries. *Energy Environ. Sci.* **2019**, *12*, 3203−3224.

(2) Randau, S.; Weber, D. A.; Koetz, O.; Koerver, R.; Braun, P.; Weber, A.; Ivers-Tiffée, E.; Adermann, T.; Kulisch, J.; Zeier, W. G.; Richter, F. H.; Janek, J. Benchmarking the performance of all-solid-state lithium batteries. *Nat. Energy* **2020**, *5*, 259−270.

(3) Zhang, X.; Wang, S.; Xue, C. J.; Xin, C. Z.; Lin, Y. H.; Shen, Y.; Li, L. L.; Nan, C. W. Self-suppression of lithium dendrite in all-solid-state lithium metal batteries with poly(vinylidene difluoride)-based solid electrolytes. *Adv. Mater.* **2019**, *31*, 1806082.

(4) Wang, X. E.; Chen, F. F.; Girard, G. M. A.; Zhu, H. J.; MacFarlane, D. R.; Mecerreyes, D.; Armand, M.; Howlett, P. C.; Forsyth, M. Poly(ionic liquid)s-in-salt electrolytes with Co-coordination-assisted lithium-ion transport for safe batteries. *Joule* **2019**, *3*, 2687−2702.

(5) Zou, J. Y.; Trewin, A.; Ben, T.; Qiu, S. L. High uptake and fast transportation of $LiPF_6$ in a porous aromatic framework for solid-state Li-ion batteries. *Angew. Chem.* **2020**, *132*, 779−784.

(6) Zhang, H.; Oteo, U.; Zhu, H. J.; Judez, X.; Martinez-Ibañez, M.; Aldalur, I.; Sanchez-Diez, E.; Li, C. M.; Carrasco, J.; Forsyth, M.; Armand, M. Enhanced Lithium-Ion Conductivity of Polymer Electrolytes by Selective Introduction of Hydrogen into the Anion. *Angew. Chem., Int. Ed.* **2019**, *58*, 7829−7834.

(7) Jaumaux, P.; Liu, Q.; Zhou, D.; Xu, X. F.; Wang, T. Y.; Wang, Y. Z.; Kang, F. Y.; Li, B. H.; Wang, G. X. Deep-eutectic-solvent-based self-healing polymer electrolyte for safe and long-life lithium-metal batteries. *Angew. Chem., Int. Ed.* **2020**, *59*, 9134−9142.

(8) Cui, Y.; Wan, J. Y.; Ye, Y. S.; Liu, K.; Chou, L. Y.; Cui, Y. A fireproof, lightweight, polymer-polymer solid-state electrolyte for safe lithium batteries. *Nano Lett.* **2020**, *20* (3), 1686−1692.

(9) Rosso, M.; Brissot, C.; Teyssot, A.; Dollé, M.; Sannier, L.; Tarascon, J. M.; Bouchet, R.; Lascaud, S. Dendrite short-circuit and fuse effect on Li/polymer/Li cells. *Electrochim. Acta* **2006**, *51*, 5334−5340.

(10) Zhang, Z. S.; Zhang, L.; Liu, Y. Y.; Wang, H. Q.; Yu, C.; Zeng, H.; Wang, L. M.; Xu, B. Interface-engineered $Li_7La_3Zr_2O_{12}$-based garnet solid electrolytes with suppressed Li-dendrite formation and enhanced electrochemical performance. *ChemSusChem* **2018**, *11*, 3774−3782.

(11) Dai, J. Q.; Yang, C. P.; Wang, C. W.; Pastel, G.; Hu, L. B. Interface engineering for garnet-based solid-state lithium-metal batteries: materials, structures, and characterization. *Adv. Mater.* **2018**, *30*, 1802068.

(12) Zhang, F. Z.; Huang, Q. A.; Tang, Z. P.; Li, A. J.; Shao, Q. S.; Zhang, L.; Li, X. F.; Zhang, J. J. A review of mechanics-related material damages in all-solid-state batteries: mechanisms, performance impacts and mitigation strategies. *Nano Energy* **2020**, *70*, 104545.

(13) Xu, L.; Tang, S.; Cheng, Y.; Wang, K. Y.; Liang, J. Y.; Liu, C.; Cao, Y. C.; Wei, F.; Mai, L. Q. Interfaces in solid-state lithium batteries. *Joule* **2018**, *2*, 1991−2015.

(14) Gao, Y.; Wang, D. W.; Li, Y. C.; Yu, Z. X.; Mallouk, T. E.; Wang, D. H. Salt-based organic-inorganic nanocomposites: towards a stable lithium metal/$Li_{10}GeP_2S_{12}$ solid electrolyte interface. *Angew. Chem., Int. Ed.* **2018**, *57*, 13608−13612.

(15) Wang, C. W.; Fu, K.; Kammampata, S. P.; McOwen, D. W.; Samson, A. J.; Zhang, L.; Hitz, G. T.; Nolan, A. M.; Wachsman, E. D.; Mo, Y. F.; Thangadurai, V.; Hu, L. B. Garnet-type solid-state electrolytes: materials, interfaces, and batteries. *Chem. Rev.* **2020**, *120*, 4257−4300.

(16) Zhang, X. Y.; Xiang, Q.; Tang, S.; Wang, A. X.; Liu, X. J.; Luo, J. Y. Long cycling life solid-state Li metal batteries with stress self-adapted Li/garnet interface. *Nano Lett.* **2020**, *20* (4), 2871−2878.

(17) Ma, C.; Cheng, Y. Q.; Yin, K. B.; Luo, J.; Sharafi, A.; Sakamoto, J.; Li, J. C.; More, K. L.; Dudney, N. J.; Chi, M. F. Interfacial stability of Li metal-solid electrolyte elucidated via in situ electron microscopy. *Nano Lett.* **2016**, *16* (11), 7030−7036.

(18) Xu, H. H.; Li, Y. T.; Zhou, A. J.; Wu, N.; Xin, S.; Li, Z. Y.; Goodenough, J. B. Li_3N-modified garnet electrolyte for all-solid-state lithium metal batteries operated at 40 degrees C. *Nano Lett.* **2018**, *18* (11), 7414−7418.

(19) Chen, X. Z.; He, W. J.; Ding, L. X.; Wang, S. Q.; Wang, H. H. Enhancing interfacial contact in all solid state batteries with a cathode-supported solid electrolyte membrane framework. *Energy Environ. Sci.* **2019**, *12*, 938−944.

(20) Cao, X.; Ren, X. D.; Zou, L. F.; Engelhard, M. H.; Huang, W.; Wang, H. S.; Matthews, B. E.; Lee, H.; Niu, C. J.; Arey, B. W.; Cui, Y.; Wang, C. M.; Xiao, J.; Liu, J.; Xu, W.; Zhang, J. G. Monolithic solid-electrolyte interphases formed in fluorinated orthoformate-based electrolytes minimize Li depletion and pulverization. *Nat. Energy* **2019**, *4*, 796−805.

(21) Chi, S. S.; Liu, Y. C.; Zhao, N.; Guo, X. X.; Nan, C. W.; Fan, L. Z. Solid polymer electrolyte soft interface layer with 3D lithium anode for all-solid-state lithium batteries. *Energy Storage Mater.* **2019**, *17*, 309−316.

(22) Yan, J.; Liu, F. Q.; Hu, Z. Y.; Gao, J.; Zhou, W. D.; Huo, H.; Zhou, J. J.; Li, L. Realizing dendrite-free lithium deposition with a composite separator. *Nano Lett.* **2020**, *20* (5), 3798−3807.

(23) Yang, X. F.; Sun, Q.; Zhao, C. T.; Gao, X. J.; Adair, K. R.; Liu, Y. L.; Luo, J.; Lin, X. T.; Liang, J. N.; Huang, H.; Zhang, L.; Yang, R.; Lu, S. G.; Li, R. Y.; Sun, X. L. High-areal-capacity all-solid-state lithium batteries enabled by rational design of fast ion transport channels in vertically-aligned composite polymer electrodes. *Nano Energy* **2019**, *61*, 567−575.

(24) Krauskopf, T.; Dippel, R.; Hartmann, H.; Peppler, K.; Mogwitz, B.; Richter, F. H.; Zeier, W. G.; Janek, J. Lithium-metal growth kinetics on LLZO garnet-type solid electrolytes. *Joule* **2019**, *3*, 2030−2049.

(25) Han, F. D.; Westover, A. S.; Yue, J.; Fan, X. L.; Wang, F.; Chi, M. F.; Leonard, D. N.; Dudney, N.; Wang, H.; Wang, C. S. High electronic conductivity as the origin of lithium dendrite formation within solid electrolytes. *Nat. Energy* **2019**, *4*, 187−196.

(26) Lin, D.; Liu, Y.; Cui, Y. Reviving the lithium metal anode for high-energy batteries. *Nat. Nanotechnol.* **2017**, *12*, 194−206.

(27) Yang, P.; Gao, X.; Tian, X.; Shu, C.; Yi, Y.; Liu, P.; Wang, T.; Qu, L.; Tian, B.; Li, M.; Tang, W.; Yang, B.; Goodenough, J. B. Upgrading Traditional Organic Electrolytes toward Future Lithium Metal Batteries: A Hierarchical Nano-SiO_2-Supported Gel Polymer Electrolyte. *ACS Energy Lett.* **2020**, *5* (5), 1681−1688.
(28) Xiong, X. S.; Zhou, Q.; Zhu, Y. S.; Chen, Y. H.; Fu, L. J.; Liu, L. L.; Yu, N. F.; Wu, Y. P.; van Ree, T. In pursuit of a dendrite-free electrolyte/electrode interface on lithium metal anodes: a minireview. *Energy Fuels* **2020**, *34* (9), 10503−10512.
(29) Wu, Y. Q.; Ming, H.; Li, M. L.; Zhang, J. L.; Wahyudi, W.; Xie, L. Q.; He, X. M.; Wang, J.; Wu, Y. P.; Ming, J. New Organic Complex for Lithium Layered Oxide Modification: Ultrathin Coating, High-Voltage, and Safety Performances. *ACS Energy Lett.* **2019**, *4* (3), 656−665.
(30) Ding, F.; Xu, W.; Graff, G. L.; Zhang, J.; Sushko, M. L.; Chen, X. L.; Shao, Y. Y.; Engelhard, M. H.; Nie, Z. M.; Xiao, J.; Liu, X. J.; Sushko, P. V.; Liu, J.; Zhang, J. G. Dendrite-free lithium deposition via self-healing electrostatic shield mechanism. *J. Am. Chem. Soc.* **2013**, *135*, 4450−4456.
(31) Xu, R. C.; Han, F. D.; Ji, X.; Fan, X. L.; Tu, J. P.; Wang, C. S. Interface engineering of sulfide electrolytes for all-solid-state lithium batteries. *Nano Energy* **2018**, *53*, 958−966.
(32) Bag, S.; Zhou, C. T.; Kim, P. J.; Pol, V. G.; Thangadurai, V. LiF modified stable flexible PVDF-garnet hybrid electrolyte for high performance all-solid-state Li-S batteries. *Energy Storage Mater.* **2020**, *24*, 198−207.
(33) Xiao, J.; Zhai, P. B.; Wei, Y.; Zhang, X. Y.; Yang, W. W.; Cui, S. Q.; Jin, C. Q.; Liu, W.; Wang, X. G.; Jiang, H. N.; Luo, Z. L.; Zhang, X. K.; Gong, Y. J. In-situ formed protecting layer from organic/inorganic concrete for dendrite-free lithium metal anodes. *Nano Lett.* **2020**, *20* (5), 3911−3917.
(34) Liu, Y. Y.; Lin, D. C.; Yuen, P. Y.; Liu, K.; Xie, J.; Dauskardt, R. H.; Cui, Y. An artificial solid electrolyte interphase with high Li-ion conductivity, mechanical strength, and flexibility for stable lithium metal anodes. *Adv. Mater.* **2017**, *29*, 1605531.
(35) Yuan, Y. X.; Wu, F.; Bai, Y.; Li, Y.; Chen, G. H.; Wang, Z. H.; Wu, C. Regulating Li deposition by constructing LiF-rich host for dendrite-free lithium metal anode. *Energy Storage Mater.* **2019**, *16*, 411−418.
(36) Kalogiannis, T.; Hosen, M. S.; Sokkeh, M. A.; Goutam, S.; Jaguemont, J.; Jin, L.; Qiao, G.; Berecibar, M.; Van Mierlo, J. Comparative study on parameter identification methods for dual-polarization lithium-ion equivalent circuit model. *Energies* **2019**, *12* (21), 4031.
(37) Wu, N.; Chien, P. H.; Qian, Y. M.; Li, Y. T.; Xu, H. H.; Grundish, N. S.; Xu, B. Y.; Jin, H. B.; Hu, Y. Y.; Yu, G. H.; Goodenough, J. B. Enhanced surface interactions enable fast Li^+ conduction in oxide/polymer composite electrolyte. *Angew. Chem., Int. Ed.* **2020**, *59*, 4131−4137.
(38) Lau, J.; DeBlock, R. H.; Butts, D. M.; Ashby, D. S.; Choi, C. S.; Dunn, B. S. Sulfide solid electrolytes for lithium battery applications. *Adv. Energy Mater.* **2018**, *8*, 1800933.
(39) Zheng, J.; Tang, M. X.; Hu, Y. Y. Lithium ion pathway within $Li_7La_3Zr_2O_{12}$-polyethylene oxide composite electrolytes. *Angew. Chem.* **2016**, *128*, 12726−12730.
(40) Wu, X. H.; Villevieille, C.; Novak, P.; El Kazzi, M. Insights into the chemical and electronic interface evolution of $Li_4Ti_5O_{12}$ cycled in Li_2S-P_2S_5 enabled by operando X-ray photoelectron spectroscopy. *J. Mater. Chem. A* **2020**, *8*, 5138−5146.
(41) Wood, K. N.; Teeter, G. XPS on Li-battery-related compounds: analysis of inorganic SEI phases and a methodology for charge correction. *ACS Appl. Energy Mater.* **2018**, *1*, 4493−4504.
(42) Chen, X. R.; Yao, Y. X.; Yan, C.; Zhang, R.; Cheng, X. B.; Zhang, Q. A diffusion-reaction competition mechanism to tailor lithium deposition for lithium-metal batteries. *Angew. Chem.* **2020**, *132*, 7817−7821.
(43) Zhang, R.; Chen, X. R.; Chen, X.; Cheng, X. B.; Zhang, X. Q.; Yan, C.; Zhang, Q. Lithiophilic sites in doped graphene guide uniform lithium nucleation for dendrite-free lithium metal anodes. *Angew. Chem., Int. Ed.* **2017**, *56*, 7764−7768.
(44) Yasin, G.; Arif, M.; Mehtab, T.; Lu, X.; Yu, D. L.; Muhammad, N.; Nazir, M. T.; Song, H. Understanding and suppression strategies toward stable Li metal anode for safe lithium batteries. *Energy Storage Mater.* **2020**, *25*, 644−678.
(45) Ahamad, S.; Gupta, A. Understanding composition and morphology of solid-electrolyte interphase in mesocarbon microbeads electrodes with nano-conducting additives. *Electrochim. Acta* **2020**, *341*, 136015.
(46) Tian, Y. F.; Zheng, H. Y.; Zhang, L. L.; Chi, B.; Pu, J.; Li, J. Direct electrolysis of CO_2 in symmetrical solid oxide electrolysis cell based on $La_{0.6}Sr_{0.4}Fe_{0.8}Ni_{0.2}O_{3-\delta}$ electrode. *J. Electrochem. Soc.* **2018**, *165* (2), F17−F23.
(47) Zhang, J.; Zheng, C.; Li, L. J.; Xia, Y.; Huang, H.; Gan, Y. P.; Liang, C.; He, X. P.; Tao, X. Y.; Zhang, W. K. Lithium batteries: unraveling the intra and intercycle interfacial evolution of Li_6PS_5Cl-based all-solid-state lithium batteries. *Adv. Energy Mater.* **2020**, *10*, 1903311.
(48) Swamy, T.; Chen, X. W.; Chiang, Y. M. Electrochemical redox behavior of Li ion conducting sulfide solid electrolytes. *Chem. Mater.* **2019**, *31*, 707−713.
(49) Manuel Stephan, A.; Gopu Kumar, S.; Renganathan, N.G.; Anbu Kulandainathan, M. Characterization of poly (vinylidene fluoride−hexafluoropropylene)(PVdF-HFP) electrolytes complexed with different lithium salts. *Eur. Polym. J.* **2005**, *41*, 15−21.
(50) Aguesse, F.; Manalastas, W.; Buannic, L.; Lopez del Amo, J. M.; Singh, G.; Llordes, A.; Kilner, J. Investigating the dendritic growth during full cell cycling of garnet electrolyte in direct contact with Li metal. *ACS Appl. Mater. Interfaces* **2017**, *9*, 3808−3816.
(51) Song, Y. L.; Yang, L. Y.; Zhao, W. G.; Wang, Z. J.; Zhao, Y.; Wang, Z. Q.; Zhao, Q. H.; Liu, H.; Pan, F. Solid-State Electrolytes: revealing the short-circuiting mechanism of garnet-based solid-state electrolyte. *Adv. Energy Mater.* **2019**, *9*, 1900671.
(52) Zhang, H. T.; Wang, D. Y.; Shen, C. In-situ EC-AFM and ex-situ XPS characterization to investigate the mechanism of SEI formation in highly concentrated aqueous electrolyte for Li-ion batteries. *Appl. Surf. Sci.* **2020**, *507*, 145059.
(53) Lin, Z.; Liu, Z. C.; Dudney, N. J.; Liang, C. D. Lithium superionic sulfide cathode for all-solid lithium−sulfur batteries. *ACS Nano* **2013**, *7* (3), 2829−2833.
(54) Cheng, X. B.; Yan, C.; Peng, H. J.; Huang, J. Q.; Yang, S. T.; Zhang, Q. Sulfurized solid electrolyte interphases with a rapid Li^+ diffusion on dendrite-free Li metal anodes. *Energy Storage Mater.* **2018**, *10*, 199−205.
(55) Lepley, N. D.; Holzwarth, N. A. W.; Du, Y. J. A. Structures, Li^+ mobilities, and interfacial properties of solid electrolytes Li_3PS_4 and Li_3PO_4 from first principles. *Phys. Rev. B: Condens. Matter Mater. Phys.* **2013**, *88*, 104103.
(56) Xiong, K.; Longo, R.C.; KC, S.; Wang, W.; Cho, K. Behavior of Li defects in solid electrolyte lithium thiophosphate $Li_7P_3S_{11}$: A first principles study. *Comput. Mater. Sci.* **2014**, *90*, 44−49.
(57) Zhang, Y.; Zuo, T. T.; Popovic, J.; Lim, K.; Yin, Y. X.; Maier, J.; Guo, Y. G. Towards better Li metal anodes: challenges and strategies. *Mater. Today* **2020**, *33*, 56−74.
(58) Wang, D.; Zhang, W.; Zheng, W. T.; Cui, X. Q.; Rojo, T.; Zhang, Q. Towards high-safe lithium metal anodes: suppressing lithium dendrites via tuning surface energy. *Adv. Sci.* **2017**, *4*, 1600168.

https://dx.doi.org/10.1021/acs.nanolett.0c03395
Nano Lett. 2020, 20, 8273−8281